Journal of Translational Medicine

RESEARCH

Open Access

F-box protein FBXO21 overexpression inhibits the proliferation and metastasis of clear cell renal cell carcinoma and is closely related to the CREB pathway and tumor immune cell infiltration

Wuping Yang[1], Taile Jing[1], Cunjin Wu[1], Minghao Lu[1], Xiaolin Yao[1], Dan Xia[1*] and Ding Peng[1*]

Abstract

Background Many studies have shown that F-box proteins regulate epithelial-mesenchymal transition, which is closely related to tumor metastasis. However, there is still limited research on the role of F-box proteins in renal cell carcinoma (RCC).

Methods Public databases were used to screen differentially expressed genes among 37 F-box proteins in clear cell RCC (ccRCC). The expression of the differential gene FBXO21 and its prognostic value were verified by RT-qPCR and immunohistochemistry. Pyrosequencing was used to detect the regulatory effect of DNA methylation on FBXO21 expression. The effects of FBXO21 expression on cell proliferation and metastasis were clarified through cell phenotype experiments and animal models. The relationship between FBXO21 expression and the infiltration levels of tumor immune cells was also analyzed. GSEA and Western blot were used to identify the downstream molecular pathways associated with FBXO21 expression.

Results Our results revealed that FBXO21 was significantly underexpressed in ccRCC and that increased FBXO21 expression predicted a better patient prognosis. The promoter region of FBXO21 exhibited DNA hypermethylation, and FBXO21 expression was significantly restored after demethylation. In addition, FBXO21 overexpression significantly inhibited the proliferation and metastasis of ccRCC cells both in vitro and in vivo. Mechanistically, FBXO21 expression was related to the stroma score and the infiltration levels of immune infiltrating cells associated with prognosis. Moreover, FBXO21 overexpression increased the expression of key molecules in the CREB pathway.

Conclusions These results suggest that FBXO21 is a novel prognostic biomarker for ccRCC patients and functions as a tumor suppressor gene. Moreover, FBXO21 may regulate the CREB pathway and is closely related to tumor immune cell infiltration in ccRCC.

Keywords FBXO21, CcRCC, DNA hypermethylation, Tumor immunes infiltrating cells, CREB pathway

*Correspondence:
Dan Xia
xiaxy1998@163.com
Ding Peng
ding_peng@zju.edu.cn

Background

Renal cell carcinoma (RCC), one of the most common malignancies of the urinary system, was estimated to be responsible for 434,419 new cases and 155,702 deaths in 185 countries in 2022 [1]. In 2024, RCC ranked sixth and ninth in the number of new cases of all types of cancer among men and women in the United States, respectively [2]. Among RCCs, clear cell RCC (ccRCC) is the most common subtype, accounting for more than 75% of all RCCs, and is also a significant contributor to cancer-related death in patients [3]. Although early localized RCC patients have a better prognosis with surgical treatment, approximately one-third of patients have already developed metastasis upon diagnosis, with a 5-year survival rate of less than 15% [4–7]. Therefore, RCC is a serious threat to human life worldwide. In the past two decades, targeted treatment with vascular endothelial growth factor (VEGF) has been the main treatment method for metastatic RCC (mRCC), but its efficacy is still low and it is prone to drug resistance [8]. Although the emergence of immune checkpoint inhibitors has improved the survival rate of patients to some extent, only a portion of patients have achieved significant and lasting benefits, and their effectiveness still needs to be further improved [9–11]. Therefore, it is urgent to find more effective and safe therapeutic targets to improve the prognosis of RCC patients, especially mRCC patients.

-box proteins are the recognition subunits of the polymeric E3 ubiquitin ligase complex involved in the degradation of specific substrates by the proteasome. Over the past few years, discrete quantities of F-box proteins have been shown to regulate epithelial-mesenchymal transition (EMT), which is closely associated with tumor metastasis [12]. For example, FBXO11 expression is upregulated in gastric cancer tissue, and silencing FBXO11 weakens the proliferation, migration, and invasion ability of cancer cells, whereas FBXO11 overexpression promotes the EMT process of cancer cells [13]. FBXO22 is upregulated in primary breast tumors and promotes cell proliferation, colony formation, EMT, and cell motility in vitro while promoting the tumorigenicity of xenografts and metastatic lung colonization in vivo [14]. FBXO31 is expressed at low levels in cervical cancer tissues and cell lines, and the overexpression of FBXO31 inhibits tumor cell survival, invasion, migration, and EMT and induced apoptosis [15]. FBXO32 is overexpressed in lung adenocarcinoma, and its increased expression is associated with poor patient prognosis and promotes the invasion and metastasis of lung adenocarcinoma cells both in vitro and in vivo [16]. Thus, F-box proteins may play different important roles in various tumors and are closely related to tumor metastasis.

Previous studies have also reported that some F-box proteins may play important roles in RCC. For example, an analysis of the Oncomine public database revealed that the FBXO11 mRNA level in normal tissues was lower than that in RCC tissues and that the expression of FBXO11 in metastatic lesions was significantly greater than that in primary lesions and was associated with poor prognosis in ccRCC patients [17]; moreover, the FBXO30 expression level was lower in ccRCC tissues than in adjacent normal tissues, which inhibited the tumorigenesis and metastasis ability of ccRCC cells both in vivo and in vitro [18]. Thus, the role of F-box proteins in RCC cannot be ignored.

In this study, we previously analysed the expression of 37 F-box proteins in public databases and validated them via clinical samples from our center. Our results revealed that FBXO21 expression was significantly reduced in ccRCC patients and that increased FBXO21 expression was closely related to a better patient prognosis. However, there is currently no research on FBXO21 in RCC. Thus, more studies are needed to clarify the expression characteristics, biological functions, and upstream and downstream regulatory mechanisms of FBXO21 in RCC.

Materials and methods

Public database

The expression data of FBXO21 mRNA in 538 ccRCC and 72 adjacent normal renal (AN) tissues were obtained from the TCGA-KIRC (The Cancer Genome Atlas-Kidney Renal Clear Cell Carcinoma) public database, of which 530 patients had detailed prognosis and tumor pathological characteristics information. The expression data of FBXO21 in ccRCC and their AN tissues in 9 GSE datasets (GSE40435, GSE53757, GSE66272, GSE68417, GSE105261, GSE73731, GSE126964, GSE166734, and GSE168845) were obtained from the GEO (Gene Expression Omnibus) public database.

In addition, the DNA methylation data of FBXO21 in 325 tumor and 160 AN tissues were obtained from the TCGA-KIRC database, of which 317 patients had detailed prognostic and tumor pathological characteristic information. The DNA methylation data of 4 CpG sites (cg00603363, cg01817067, cg12414070 and cg26470309) in 3 GSE datasets (GSE61441, GSE70303, and GSE105260) were also obtained.

Furthermore, the immune score, stroma score, microenvironment score, and the infiltration data of 36 types of immune cells from 530 ccRCC patients in the TCGA-KIRC cohort were obtained from the TIMER database. The names of these 36 types of immune cells are as follows: Myeloid dendritic cell activated, B cell, T cell CD4+memory, T cell CD4+naive, T cell CD4+(non-regulatory), T cell CD4+central memory,

T cell CD4 + effector memory, T cell CD8 + naive, T cell CD8 + , T cell CD8 + central memory, T cell CD8 + effector memory, Class-switched memory B cell, Common lymphoid progenitor, Common myeloid progenitor, Myeloid dendritic cell, Endothelial cell, Eosinophil, Cancer associated fibroblast, Granulocyte-monocyte progenitor, Hematopoietic stem cell, Macrophage, Macrophage M1, Macrophage M2, Mast cell, B cell memory, Monocyte, B cell naive, Neutrophil, NK cell, T cell NK, Plasmacytoid dendritic cell, B cell plasma, T cell gamma delta, T cell CD4 + Th1, T cell CD4 + Th2, T cell regulatory (Tregs).

Tissue sample acquisition and cell culture

All tissue samples from patients were obtained from the Department of Urology, the First Affiliated Hospital, Zhejiang University School of Medicine, after they signed the informed consent form (Ethical approval number: 2024 Research No. 0921). We conducted a 3-year collection of 120 pairs of fresh ccRCC and AN (adjacent normal) tissue samples from January 2014 to December 2016, with some samples used for paraffin embedding and others frozen in liquid nitrogen. In addition, the patients were followed up for a period of 7 years from January 2017 to December 2023. Among these samples, 24 pairs of ccRCC and AN tissue samples frozen in liquid nitrogen were used for the RT-qPCR detection of FBXO15, FBXO21, and FBXO43 mRNA; the paraffin sections of 120 pairs of ccRCC and AN tissues were used for FBXO21 protein immunohistochemical staining; 54 ccRCC and 10 AN tissue samples frozen in liquid nitrogen were utilized for pyrosequencing. The detailed sample testing information has been provided in Supplementary Table 1.

The normal control cell line HK2 and three ccRCC cell lines (786-O, OSRC2, and Caki-1) were purchased from the American Type Culture Collection (ATCC). All the cells were cultured in DMEM containing 10% fetal bovine serum in an incubator at 37 ℃ with 5% CO2.

In addition, we constructed a FBXO21 overexpression plasmid. The lentivirus was packaged in a three-plasmid system, and Lipofectamine 3000 was used as the transfection reagent. After 48 h of virus transfection, OSRC2 and Caki-1 cell lines stably transfected with FBXO21 were obtained by screening with puromycin (5 μg/ml).

RT–qPCR

TRIzol reagent was used to extract RNA from 24 pairs of ccRCC and AN tissues. Then, reverse transcription was performed to obtain cDNA samples. The specific primer sequences for RT–qPCR were as follows: (1) FBXO15: forward primer CAACGTGAGAAGGAAAGGGGC, reverse primer AGAAAGAGCTCTCCCAGTGC; (2) FBXO21: forward primer GAGGTGGCCTTCCCTTAT GAA, reverse primer CCCAGCTTTTTGCCGAACTTT A; (3) FBXO43: forward primer GAGAGCCTATGCAGT GTTTGG, reverse primer TA AAAGCTGGAGCCGAG TGG.

Immunohistochemistry

Immunohistochemical staining was used to detect the protein expression of FBXO21 in 120 ccRCC patients and their AN tissues at our center. The protein expression of N-cadherin and E-cadherin in pulmonary metastatic tumors was also examined. The detailed antibody information was as follows: FBXO21 primary antibody (ABclonal, A16107, 1:100), E-cadherin primary antibody (Abcam, ab40772, 1:500), and N-cadherin primary antibody (Abcam, ab19348, 1:1000). In addition, the relationships between FBXO21 expression and tumor stage, grade, metastasis status, and patient prognosis were further analysed by combining the pathological features of these 120 tumors with the survival information of patients.

Immunofluorescence

An FBXO21 antibody (ABclonal, A16107, 1:100) was used for immunofluorescence staining, and images were captured via confocal laser scanning microscopy to clarify the sublocalization of the FBXO21 protein in ccRCC cells. In addition, since mitochondria are evenly distributed in the cytoplasm in most cells, we used the TOMM20 protein located on the outer membrane of the mitochondria as a cytoplasmic marker.

Pyrosequencing

The methylation level of cg12414070 in ccRCC tissues and cell lines was detected by pyrosequencing. The specific primer sequences for cg12414070 were as follows: forward primer TGTTAAGTTGAGGGGGTGT, reverse primer CCAACAAACCAAAACTTAAAACCACAT CAA, and sequencing primer GTGGTTTTTTTTTAT GAAATATTA T.

Demethylation analysis

5-Azacytidine (5-Aza) is a specific methyltransferase inhibitor that reduces DNA methylation by covalently binding to DNA methyltransferase to decrease its biological activity. In this study, to clarify the regulatory effect of DNA methylation on FBXO21 expression, we used 5-Aza to inhibit the methylation level of ccRCC cells and observed changes in FBXO21 protein expression. First, we dissolved 5-Aza (Sigma Aldrich) in DMSO to a concentration of 5 mM and then divided the mixture and froze it. 786-O, OSRC2, and Caki-1 cells were subsequently seeded in six-well plates, and 5-Aza was added to the cell culture medium to a final concentration of 5 μM. After four days of cultivation, the cells were collected to

isolate DNA for DNA methylation analysis, and protein was extracted for Western blot analysis.

Western blot

Total protein was extracted from cells via RIPA lysis buffer, and the total protein level was quantified via the BCA method. The primary antibodies used were as follows: anti-FBXO21 (ABclonal, A16107, 1:100), anti-CREB1 (Proteintech, 12,208–1-AP, 1:2000), anti-SOS1 (Proteintech, 55,041–1-AP, 1:1000), anti-CAMK2D (Proteintech, 81,014–1-RR, 1:5000), anti-PRKACB (Proteintech, 55,382–1-AP, 1:1000), anti-MAPK1 (Abcam, ab231085, 1:1000), anti-PRKAR2A (Proteintech, 10,1422-AP, 1:1000), anti-PRKAR1A (Proteintech, 20,358–1-AP, 1:1000), and anti-GAPDH (Proteintech, 60,004-1-Ig, 1:8000).

EdU cell proliferation detection

The proliferation ability of ccRCC cells was detected via both the BeyoClick™ EdU-647 Cell Proliferation Detection Kit (fluorescence method) and the BeyoClick™ EdU Cell Proliferation Detection Kit (DAB method).

Cell colony formation experiment

Approximately 2×102 OSRC2 and 3×102 Caki-1 cells were seeded in 6-well plates. After 2–3 weeks of culture, the cells were stained with 0.5% crystal violet for 30 min, the plates were scanned, and the number of cell colonies was calculated.

TUNEL cell apoptosis detection

The apoptosis of ccRCC cells was detected via both a one-step TUNEL cell apoptosis detection kit (green fluorescence) and a TUNEL cell apoptosis detection kit (DAB method).

Detection of cell migration and invasion ability

For the cell migration assay, approximately 3×103 OSRC2 and 2×103 Caki-1 cells were plated into the upper chambers with 100 μL of serum-free 1640 cell culture medium, and the lower chambers were filled with 700 μL of 1640 cell culture medium containing 20% FBS. After 48 h of cultivation, the cells below the surface of the lower chamber were washed with PBS and then stained with 0.5% crystal violet for 30 min. For the cell invasion assay, except for the need to coat the upper chamber with 100 μL of Matrigel (diluted 1:7 in PBS), the other steps were the same as those described above. Finally, images were collected under an inverted microscope, and the number of cells on the lower surface was counted.

Animal experiments

Eighteen 5-week-old male BALB/c nude mice were purchased from Vitalriver Company and randomly divided into two groups to construct a subcutaneous tumor model. Approximately 2×106 FBXO21-overexpressing OSRC2 cells and their corresponding control cells were implanted subcutaneously into the right side of each mouse. The growth of subcutaneous tumors was regularly monitored, the mice were euthanized two months later to collect tumor samples, and their weights were calculated. To further detect the proliferation of cells in the subcutaneous tumors of the mice, ethynyl-2-deoxyuridine (EdU, 50 mg/kg) was intraperitoneally injected 3 h before the mice were euthanized.

Tumor cells have a certain ability to invade and metastasize, and the injection of tumor cells into the blood system of immunodeficient mice can better simulate the situation of tumor cells leaving the primary site and entering the blood circulation. Then, the ability of tumor cells to metastasize can be judged by observing the formation of metastases in distant organs (lung, liver, etc.). In addition, this model was successfully applied in our previous studies to investigate the distant metastasis ability of RCC cells [19]. In this study, eight 6-week-old male B-NDG severely immunodeficient mice were purchased from Biocytogen Company and randomly divided into two groups to construct a tumor lung metastasis model. Approximately 5×105 FBXO21-overexpressing-Luc Caki-1 cells and their corresponding control cells were suspended in 200 μl of DMEM and then injected into the lateral tail veins of the mice. Bioluminescence imaging was regularly performed on each mouse according to previous methods [20], after which the mice were euthanized after one month, and lung tissue was collected. The procedures used for the animal experiments were approved by the Animal Care and Use Committee of the First Affiliated Hospital, Zhejiang University School of Medicine, Hangzhou, China (Ethical approval number: 2024 Research No. 1278).

Gene set enrichment analysis (GSEA)

Patients were divided into a high-expression group and a low-expression group for GSEA. FDR q values less than 0.25 and P values less than 0.05 were considered to indicate analytical significance.

Statistical analyses

Student's t test and the nonparametric Mann–Whitney test were used to detect differences in continuous variables. Survival curves for patients were plotted via the Kaplan–Meier method, and the log-rank test was performed for statistical analysis. The correlations of

FBXO21 expression with the methylation levels of its CpG sites and the infiltration levels of tumor immune cells were examined via Pearson's correlation analysis. All the statistical tests were two-sided, and a P value of < 0.05 was considered to indicate a significant difference.

Results

The expression characteristics and prognostic value of F-box proteins in ccRCC based on TCGA-KIRC data

First, to preliminarily clarify the expression patterns of F-box proteins in ccRCC, we obtained the mRNA expression data of 37 proteins from the TCGA-KIRC database and compared their expression differences between ccRCC and adjacent normal (AN) tissues. Our analysis revealed that compared with those in AN tissues, FBXO-2, −3, −7–11, −15, −21, −25, −30, −33, −34, −36, −40, and −44 were significantly downregulated in ccRCC tissues, whereas FBXO-4–6, −17, −22, −28, −31, −32, −38, −39, −41–43, −45, −46, and −48 were significantly upregulated in ccRCC tissues (Supplementary Fig. 1A and B).

By combining the overall survival (OS) of ccRCC patients for prognostic analysis, the K-M survival curve analysis results revealed that the expression of FBXO-3, −6–9, −11, −15, −17, −21, −25, −28, −30, −31, −33, −34, −36, −38, −41–44, and −48 was closely related to the OS of patients. Compared with those in the relatively low-expression groups, the OS times of patients in the high-expression groups of FBXO-3, −7–9, −11, −15, −17, −21, −25, −28,−30, −31, −33, −34, −36, −38, −42, −44, and −48 were longer, whereas the OS times of patients in the high-expression groups of FBXO-6, −41, and −43 were shorter than those in the relatively low-expression groups (Supplementary Fig. 2). Besides, by combining the RFS (recurrence-free survival) of ccRCC patients for prognostic analysis, survival curve analysis revealed that the expression of FBXO-3, −6–11, −15, −17, −21, −28, −30, −31, −33, −34, −36, −38, −42, −44, and −48, was closely related to the RFS of patients. Increased expression of FBXO-3, −7–11, −15, −17, −21, −28, −30, −31, −33, −34, −36, −38, −42, −44, and −48 was associated with longer RFS, whereas decreased FBXO6 expression was associated with longer RFS (Supplementary Fig. 3).

In addition, the univariate Cox regression analysis for OS revealed that increased FBXO-3, −7–9, −11, −15, −21, −25, −30, −33, −34, and −36 expression and decreased FBXO-41 and −43 expression were associated with improved OS in patients, and the subsequent multivariate Cox regression analysis results indicated that FBXO-15, −21, and −43 expression were independent predictors of OS (Table 1). In addition, the univariate Cox regression analysis for RFS revealed that increased FBXO-3, −7–9, −11, −15, −21, −30, −33, −34, −36, and −44 expression was associated with better RFS in patients, and the multivariate Cox regression analysis results indicated that FBXO15 was an independent predictor of RFS (Table 2).

Table 1 Univariate and multivariate Cox regression analyses of OS in TCGA ccRCC patients

Parameters	Univariate analysis				Multivariate analysis			
	P	HR	95%CI		P	HR	95%CI	
			Lower	Upper			Lower	Upper
FBXO3	8.28E-08	0.5545	0.447	0.6879	0.50679	0.8075	0.4296	1.518
FBXO6	0.057	1.259	0.9932	1.596				
FBXO7	2.81E-06	0.5576	0.4366	0.712	0.189721	1.4137	0.8426	2.3720
FBXO8	1.88E-08	0.5224	0.4166	0.6551	0.259361	0.7359	0.4318	1.2539
FBXO9	0.00323	0.7093	0.5643	0.8915	0.269298	1.3242	0.8046	2.1792
FBXO11	0.000279	0.7272	0.6124	0.8635	0.828325	1.044	0.7074	1.5407
FBXO15	4.12E-06	0.4888	0.3604	0.6628	**0.001263**	0.5241	0.3539	0.7762
FBXO21	2.51E-09	0.5476	0.4492	0.6675	**0.030114**	0.6872	0.4896	0.9646
FBXO25	0.0149	0.7321	0.5696	0.941	0.925633	0.988	0.7661	1.2741
FBXO30	0.00138	0.6839	0.5419	0.8632	0.295964	1.2779	0.8068	2.024
FBXO33	0.00148	0.6615	0.5126	0.8535	0.61521	0.9149	0.6467	1.2942
FBXO34	2.57E-08	0.59	0.49	0.7104	0.160231	0.7607	0.5193	1.1143
FBXO36	0.00203	0.6654	0.5137	0.8619	0.797744	1.0446	0.7484	1.458
FBXO41	0.00465	1.24	1.068	1.44	0.400273	1.0839	0.8984	1.3077
FBXO43	8.00E-09	2.559	1.86	3.522	**0.000172**	2.1558	1.4441	3.2181
FBXO44	0.14	0.83	0.648	1.063				

Bold values indicate that the molecules can independently predict patient OS

Table 2 Univariate and multivariate Cox regression analysis of RFS in TCGA ccRCC patients

Parameters	Univariate analysis				Multivariate analysis			
	P	HR	95%CI		P	HR	95%CI	
			Lower	Upper			Lower	Upper
FBXO3	2.92E-06	0.5412	0.4184	0.7	0.84168	0.9277	0.4442	1.938
FBXO6	0.2	1.205	0.906	1.602				
FBXO7	1.51E-05	0.5291	0.3965	0.7059	0.84923	0.938	0.4849	1.814
FBXO8	9.53E-05	0.5731	0.4333	0.758	0.6203	0.8468	0.4387	1.635
FBXO9	6.15E-06	0.549	0.4233	0.712	0.44155	0.7872	0.4281	1.448
FBXO10	0.25	0.7583	0.4731	1.215				
FBXO11	0.00165	0.7188	0.5852	0.8829	0.22389	1.3265	0.8413	2.092
FBXO15	3.37E-06	0.4121	0.2835	0.5989	**0.00683**	0.493	0.2953	0.823
FBXO21	0.00388	0.6967	0.5452	0.8904	0.42997	1.1565	0.806	1.659
FBXO30	0.00292	0.6575	0.4988	0.8666	0.79783	1.076	0.6142	1.885
FBXO33	0.00055	0.5808	0.4267	0.7905	0.54698	0.872	0.5585	1.362
FBXO34	1.10E-05	0.6008	0.4788	0.754	0.08389	0.6696	0.4249	1.055
FBXO36	0.00538	0.641	0.4686	0.8767	0.73222	1.0773	0.7033	1.65
FBXO44	0.00173	0.6367	0.4801	0.8445	0.26166	0.8179	0.5758	1.162

Bold value indicates that the molecule can independently predict patient RFS.

Therefore, through the analysis of the TCGA-KIRC data, the above findings preliminarily identified F-box proteins (FBXO-15, −21, and −43) with differential expression that are closely related to patient prognosis.

Relationships between FBXO-15, −21, and −43 expression and tumor pathological features on the basis of TCGA-KIRC and GEO data

By combining the pathological features of patients in the TCGA-KIRC cohort, we analysed the relationships between the expression of FBXO-15, −21, and −43 and different tumor stages and grades, tumor metastasis, and lymph node invasion. Compared with that in T1/T2, G1/G2 and stage I/II tumors, the expression of FBXO-15 and −21 was lower in T3/T4, G3/G4 and stage III/IV tumors, whereas the expression of FBXO-43 was greater (Supplementary Fig. 4A-C). Compared with those in tumors without distant metastasis (M0), in tumors with distant metastasis (M1), FBXO-15 and −21 expression was decreased, and FBXO-43 expression was increased (Supplementary Fig. 4D). Besides, compared with that in tumors without lymph node invasion (N0), FBXO-43 expression was also significantly greater in tumors with lymph node invasion (N1) (Supplementary Fig. 4E).

In addition, we validated the expression status of FBXO-15, FBXO-21, and FBXO-43 in ccRCC and their relationships with pathological features in 9 GSE datasets (GSE40435, GSE53757, GSE66272, GSE68417, GSE105261, GSE73731, GSE126964, GSE166734, and GSE168845). Our results confirmed the low expression status of FBXO-15 and −21 and the high expression status of FBXO43 in ccRCC (Supplementary Fig. 5A-C). Compared with stage I/II tumors, stage III/IV tumors presented decreased FBXO-15 and FBXO-21 expression and increased FBXO43 expression (Supplementary Fig. 5D). Compared with that in G1/G2 tumors, FBXO43 expression was increased in G3/G4 tumors (Supplementary Fig. 5E). Compared with that in tumors without distant metastasis, FBXO15 expression was lower in tumors with distant metastasis (Supplementary Fig. 5F).

Reduced FBXO21 expression was closely related to adverse pathological features and poor prognosis using clinical samples for validation

To further verify the expression of FBXO-15, FBXO-21, and FBXO-43 in ccRCC, we used RT–qPCR to detect FBXO-15, FBXO-21, and FBXO-43 expression in 24 pairs of ccRCC and AN tissues in our center. Our results revealed that FBXO21 expression was significantly lower in ccRCC tissues than in AN tissues, whereas FBXO15 and FBXO43 expression was not significantly different between cancer and AN tissues (Fig. 1A). Therefore, we focused on FBXO21 as the research object and used immunohistochemical staining to detect its protein expression level in 120 pairs of ccRCC and AN tissues. The specific clinicopathologic characteristics of these patients are shown in Table 3. Our analysis results confirmed that FBXO21 protein expression in ccRCC tissues was significantly lower than that in AN tissues (Fig. 1B). In addition, by

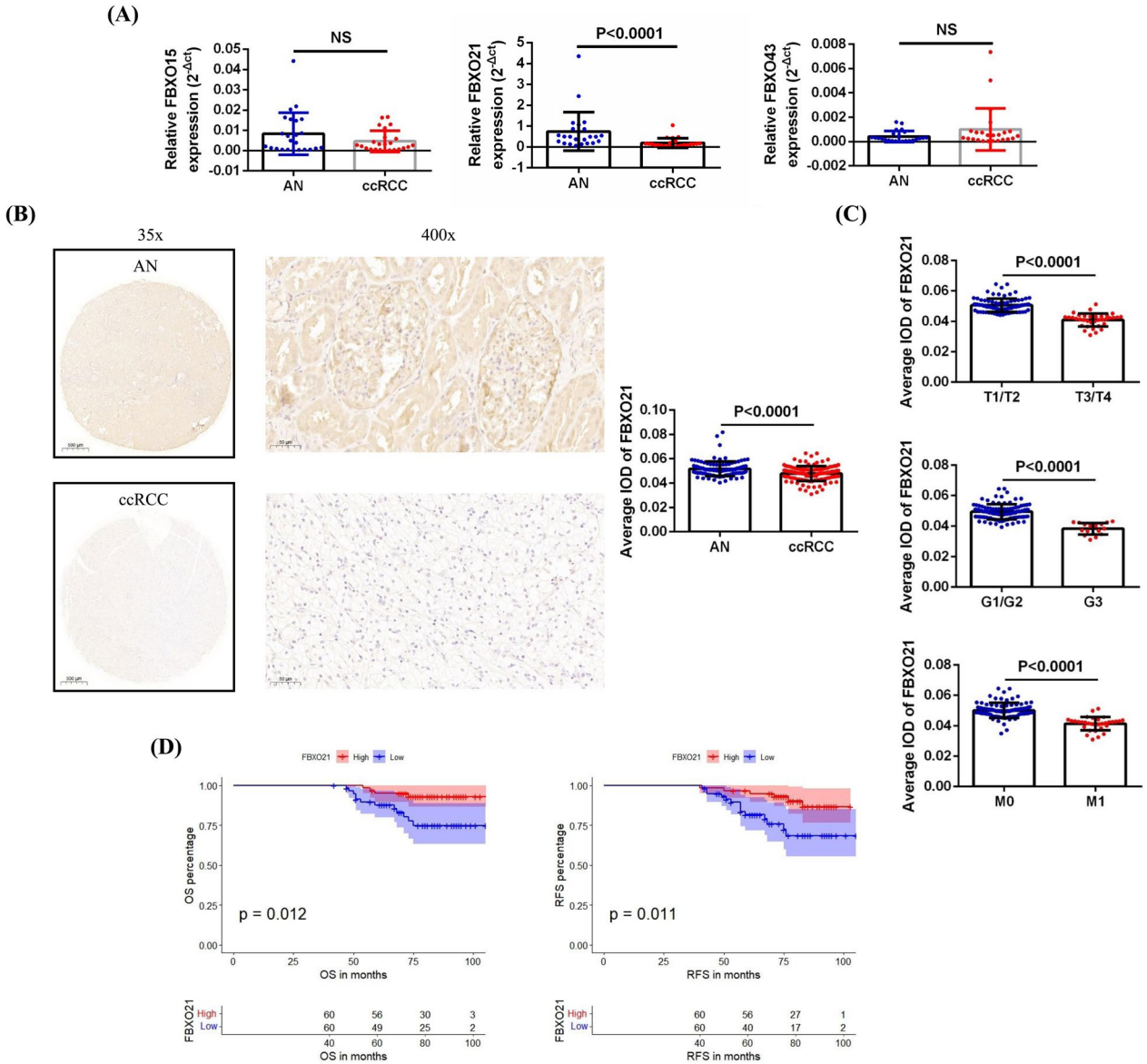

Fig. 1 Verify the expression of FBXO21 in ccRCC and its relationship with the clinical pathological characteristics and prognosis of patients. **A** RT–qPCR results of FBXO15, FBXO21, and FBXO43 mRNA expression in 24 pairs of ccRCC and AN tissues. **B** Immunohistochemical staining results of FBXO21 expression in 120 pairs of ccRCC and AN tissues. **C** Comparison of FBXO21 protein expression between T1/T2 and T3/T4 tumors, G1/G2 and G3/G4 tumors, and M0 and M1 tumors. **D** Relationship between FBXO21 protein expression and the clinical prognosis of these 120 patients. AN: adjacent normal

combining the pathological characteristics of tumors and the survival information of patients for further analysis, our results revealed that FBXO21 expression was significantly lower in advanced tumors (T3/T4, G3, and M1) than in early tumors (T1/T2, G1/G2, and M0) (Fig. 1C). Moreover, prognostic analysis revealed that patients with lower FBXO21 expression had significantly shorter OS and RFS (Fig. 1D).

Thus, our results confirmed the low expression of FBXO21 in ccRCC and that increased FBXO21 expression predicted a good prognosis for patients.

FBXO21 expression was significantly negatively correlated with its DNA methylation level

To analyse the differences in FBXO21 DNA methylation levels between ccRCC and AN tissues, methylation detection data for 27 CpG sites in FBXO21 DNA were

Table 3 The clinicopathologic characteristics of 120 ccRCC patients for validation

Clinicopathologic characteristics	n(%)
Tumor stage	
T1	51 (42.5)
T2	34 (28.3)
T3	30 (25.0)
T4	5 (4.2)
Histological grade	
G1	69 (57.5)
G2	34 (28.3)
G3	17 (14.2)
Distant metastasis	
No	88 (73.3)
Yes	32 (26.7)
Overall survival	
Alive	104 (86.7)
Dead	16 (13.3)
Replase free survival	
Non-replased	100 (83.3)
Replased	20 (16.7)

obtained from the TCGA-KIRC database (Fig. 2A). Compared with those in AN tissues, the methylation levels of 7 CpG sites (cg00603363, cg01817067, cg12414070, cg12482993, cg26376280, cg26470309, and cg26484108) were significantly increased in ccRCC tissues (Fig. 2B). The linear regression analysis results revealed that the methylation levels of 5 CpG sites (cg00603363, cg01817067, cg12414070, cg12482993, and cg26470309) were negatively correlated with FBXO21 expression (Fig. 2C). The K–M survival curve analysis results indicated that the methylation levels of 4 CpG sites (cg00603363, cg01817067, cg12414070, and cg26470309) were closely related to the prognosis of patients, and patients with higher methylation levels of these 4 CpG sites had significantly shorter OS (Fig. 2D). We further validated the relatively high methylation status of these 4 CpG sites in ccRCC via DNA methylation data from 3 GSE datasets (GSE61441, GSE70303, and GSE105260) (Fig. 2E). In addition, linear regression analysis was conducted on the data from the GSE105260 dataset, and the results revealed a significant negative correlation between the cg12414070 methylation level and the expression level of FBXO21 (Fig. 2F).

Verification of the negative regulatory effect of DNA methylation on FBXO21 expression

To further confirm the high methylation status of FBXO21 DNA in ccRCC, we used pyrosequencing to detect the methylation level of cg12414070 in 54 ccRCC and 10 AN tissues and conducted a comparative analysis. Our results confirmed that, compared with that in AN tissues, the methylation level of the cg12414070 site was significantly greater in ccRCC tissues (Fig. 3A). The representative pyrosequencing peak maps are shown in Supplementary Fig. 6. By combining the pathological characteristics of the tumors, the results confirmed that the cg12414070 methylation level was upregulated in tumors with distant metastasis and higher tumor stage and grade (Fig. 3B). A linear regression analysis of the protein expression data of FBXO21 in the same tumors revealed that FBXO21 expression was significantly negatively correlated with the methylation level of cg12414070 (Fig. 3C).

In addition, we used Western blot to detect FBXO21 protein expression in ccRCC cell lines. Our results revealed that compared with that in the normal control cell line HK2, FBXO21 expression was markedly lower in the 786-O, OSRC2, and Caki-1 cell lines (Fig. 3D). Next, the pyrosequencing results revealed that the cg12414070 methylation level was significantly greater in the 786-O, OSRC2, and Caki-1 cell lines (Fig. 3E). After treatment with the demethylating drug 5-azacytidine (5-Aza), the pyrosequencing results confirmed that the cg12414070 methylation level was significantly reduced (Fig. 3F), whereas the expression of the FBXO21 protein was significantly increased (Fig. 3G).

Thus, our results confirmed the low expression and high DNA methylation status of FBXO21 in ccRCC and revealed that DNA hypermethylation has a negative regulatory effect on FBXO21 expression.

FBXO21 overexpression inhibited the growth and metastasis of ccRCC in vitro and in vivo

To explore the effect of altered FBXO21 expression on the ccRCC cell phenotype, we successfully constructed OSRC2 and Caki-1 cell lines stably overexpressing the FBXO21 protein (Fig. 4A). To detect the effects of FBXO21 overexpression on OSRC2 and Caki-1 cell proliferation ability, we used an immunofluorescence TUNEL assay to detect the effects of FBXO21 overexpression on OSRC2 and Caki-1 cell apoptosis and a cell migration and invasion assay to detect the effects of FBXO21 overexpression on OSRC2 and Caki-1 cell metastasis ability in vitro. The results revealed that after FBXO21 overexpression, cell proliferation was significantly reduced (Fig. 4B and C), but cell apoptosis was significantly increased (Fig. 4D), and cell migration and invasion were also significantly suppressed (Fig. 4E and F).

In addition, we examined the effects of FBXO21 overexpression on the growth and metastasis of ccRCC in vivo via a subcutaneous tumor formation mouse

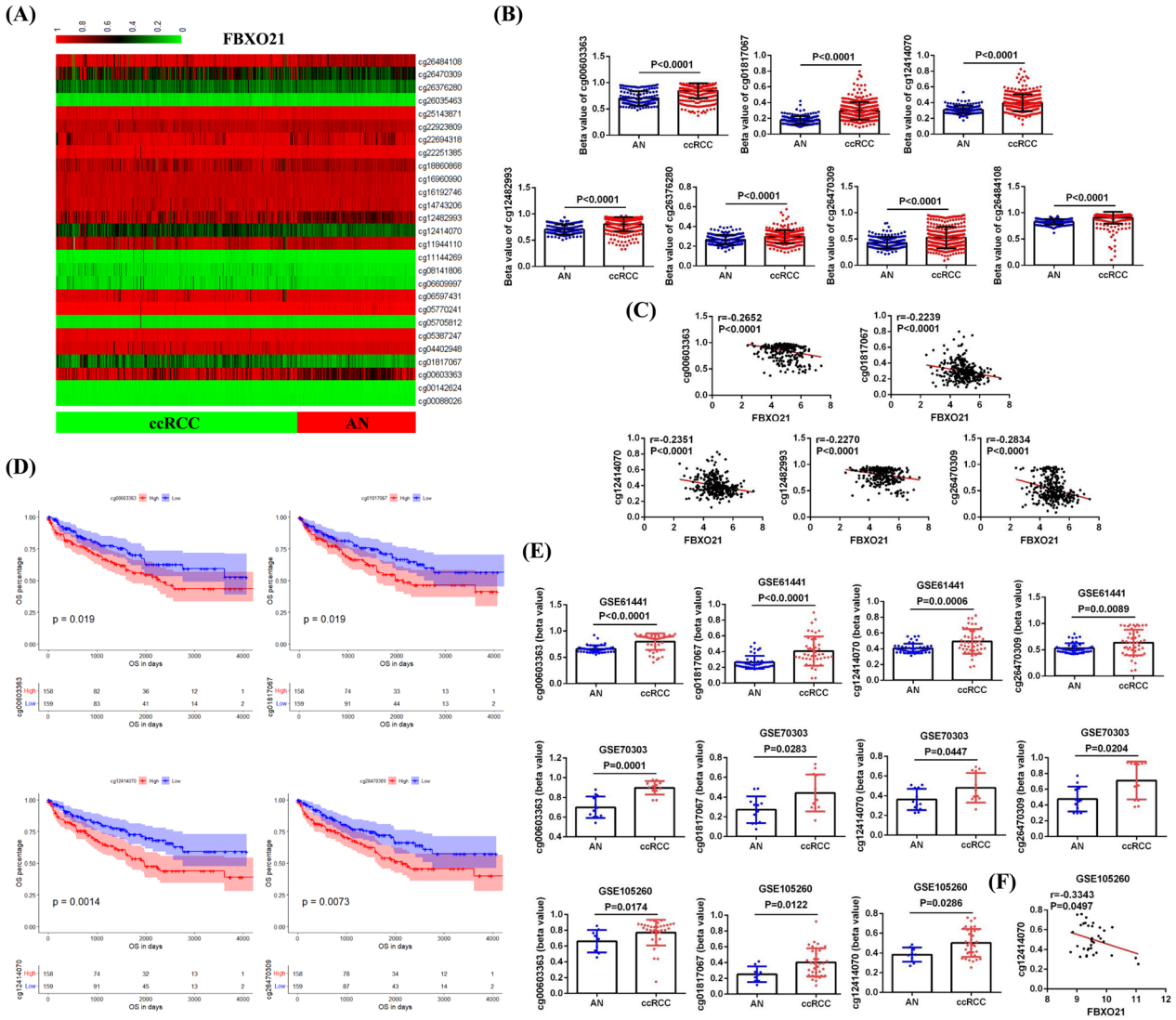

Fig. 2 Analysis of the methylation state of the CpG sites in FBXO21 DNA on the basis of TCGA-KIRC and GEO data. **A** Heatmap of the methylation levels of 27 CpG sites in FBXO21 DNA between ccRCC and AN tissues. **B** Comparison of the methylation levels of 7 CpG sites (cg00603363, cg01817067, cg12414070, cg12482993, cg26376280, cg26470309, and cg26484108) in ccRCC and AN tissues. **C** The correlation between the methylation levels of 5 CpG sites (cg00603363, cg01817067, cg12414070, cg12482993, and cg26470309) and FBXO21 expression. **D** The correlation between the methylation levels of 4 CpG sites (cg00603363, cg01817067, cg12414070, and cg26470309) and patient prognosis. **E** Verification of the methylation levels of these 4 sites in ccRCC via data from the GSE61441, GSE70303, and GSE105260 datasets. **F** Verification of the correlation between the methylation level of cg12414070 and the expression level of FBXO21 using the data from GSE105260. AN: adjacent normal

model and a lung metastasis mouse model. The lung metastasis mouse model was induced via tail vein injection of tumor cells. Our results revealed that the subcutaneous tumor weight and lung tumor luciferase signal in the FBXO21-overexpressing group were significantly lower than those in the control group (Fig. 5A and B). We subsequently used immunostaining to detect the expression of EdU and TUNEL in the paraffin sections of the subcutaneous tumors. The results confirmed that EdU expression was significantly decreased and that TUNEL expression was significantly increased in FBXO21-overexpressing tumors (Fig. 5C). Finally, H&E staining was used to detect the number of lung metastases, and immunostaining was used to examine the expression of E-cadherin (metastasis inhibition marker) and N-cadherin (metastasis facilitation marker) in the paraffin sections of the lung metastases. The results also revealed that, in the FBXO21-overexpressing group, the number of lung

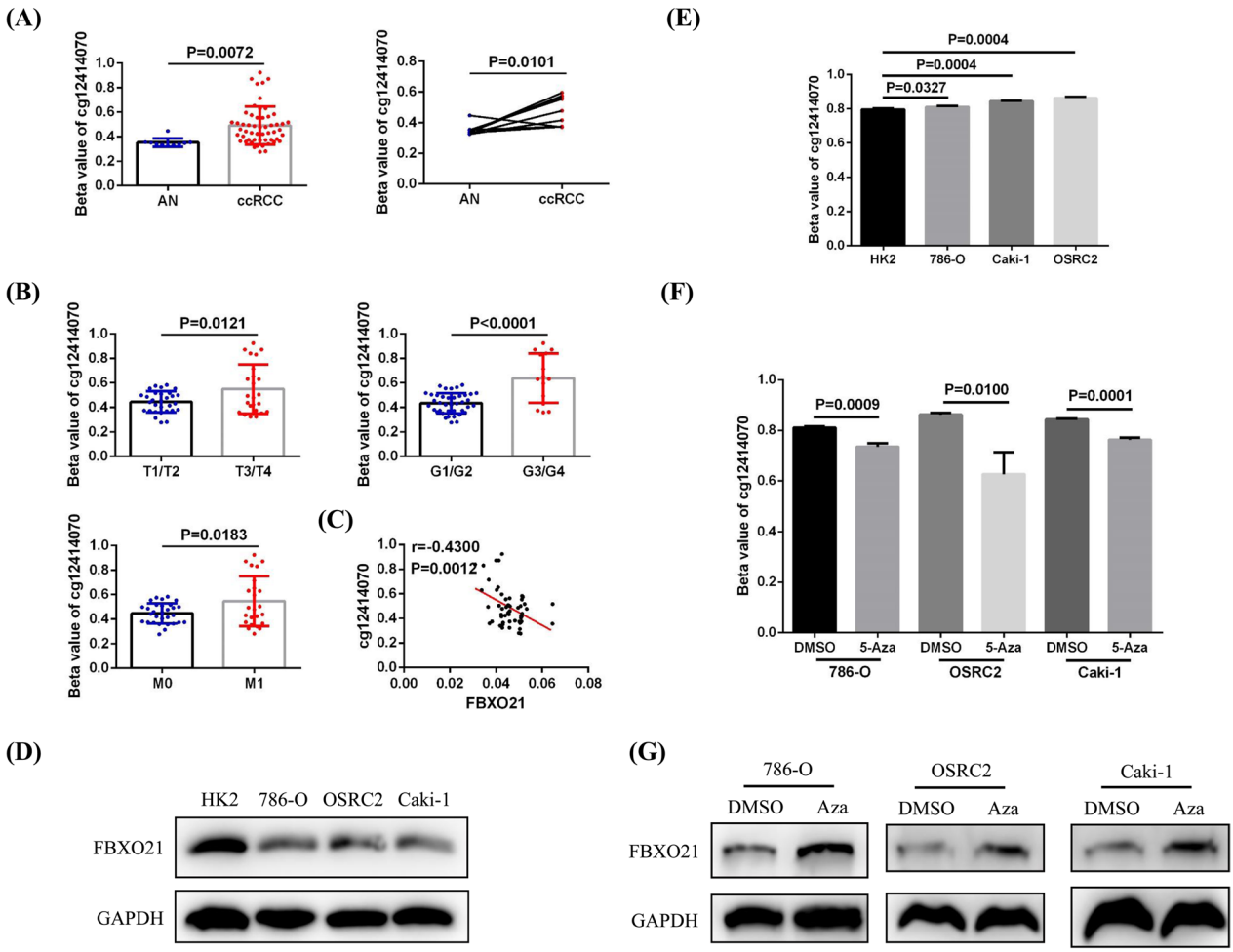

Fig. 3 Verification of the methylation level of the cg12414070 site in ccRCC and its regulatory effect on FBXO21 expression. **A** The methylation levels of cg12414070 in 54 ccRCC and 10 AN tissues were detected by pyrosequencing. **B** Comparison of the methylation level of the cg12414070 site between T1/T2 and T3/T4 tumors, G1/G2 and G3/G4 tumors, and M0 and M1 tumors. **C** The correlation between the methylation level of cg12414070 and the protein expression level of FBXO21. **D** Detection of FBXO21 protein expression in ccRCC cell lines by Western blot. **E** Detection of the methylation level of the cg12414070 site in ccRCC cell lines by pyrosequencing. **F** Detection of the methylation level of cg12414070 after treatment with demethylating drugs in ccRCC cell lines by pyrosequencing. **G** Detection of the protein expression of FBXO21 after treatment with demethylating drugs in ccRCC cell lines. AN: adjacent normal

metastases was significantly reduced (Fig. 5D), whereas E-cadherin expression was significantly increased and N-cadherin expression was significantly reduced (Fig. 5E and F).

Taken together, our above experimental results confirmed that FBXO21 overexpression significantly restrained the growth and lung metastasis ability of ccRCC cells in vitro and in vivo.

FBXO21 expression was associated with tumor immune cell infiltration and the CREB pathway in ccRCC

To explore the relationship between FBXO21 expression and tumor immune cell infiltration in ccRCC, we obtained the immune score, stroma score, microenvironment score, and infiltration data for 36 types of immune cells from the TIMER database. Prognostic analysis revealed that the stroma score and infiltration levels of 8 types of immune cells (Myeloid dendritic cell activated, B cell, Endothelial cell, Hematopoietic stem cell, Monocyte, T cell NK, B cell plasma, T cell CD4 + Th2) were associated with the OS of patients (Fig. 6A), and the infiltration levels of 6 types of immune cells (T cell CD4 + effector memory, Cancer associated fibroblast, Hematopoietic stem cell, T cell NK, B cell plasma, and T cell gamma delta) were associated with the RFS of patients (Fig. 6B). The linear regression analysis results indicated that FBXO21 expression was closely related to the stroma score

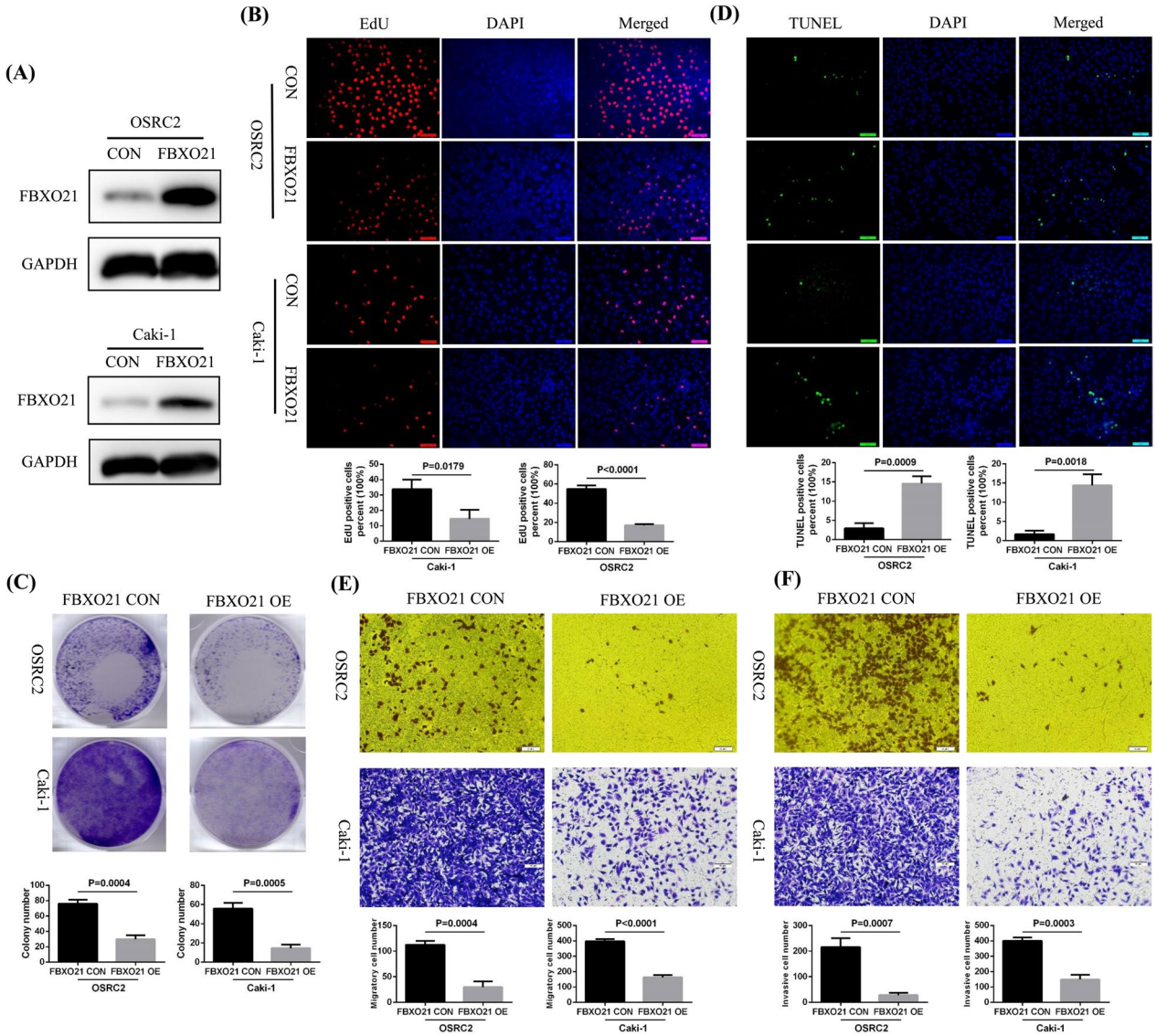

Fig. 4 Clarify the effects of FBXO21 overexpression on the proliferation, apoptosis, migration, and invasion of ccRCC cells in vitro. **A** FBXO21 was successfully overexpressed in OSRC2 and Caki-1 cell lines. **B**–**F** Effects of FBXO21 overexpression on cell proliferation (EdU marker), cell growth (colony formation), cell apoptosis (TUNEL marker), cell migration, and cell invasion

and the infiltration levels of 10 out of these 12 types of immune infiltrating cells associated with prognosis (Myeloid dendritic cell activated, B cell, T cell CD4 + effector memory, Endothelial cell, Hematopoietic stem cell, Monocyte, T cell NK, B cell plasma, T cell gamma delta, and T cell CD4 + Th2) (Fig. 6C).

In addition, we performed gene set enrichment analysis (GSEA) on the high and low expression groups of FBXO21 to investigate the potential molecular mechanism of FBXO21. The GSEA results revealed that the CREB pathway was significantly activated in the FBXO21 high-expression group (Fig. 7A). The linear regression analysis results indicated that the expression of key molecules in the CREB pathway, including RPS6KA5, PIK3CA, CREB1, SOS1, PRKAR2A, PRKACB, MAPK1, MAPK14, CAMK2D, and PRKAR1A, was significantly positively correlated with FBXO21 expression (Fig. 7B). Besides, the prognostic analysis results indicated that the expression of these 10 genes was closely related to the prognosis of patients. In the high-expression groups of RPS6KA5, PIK3CA, CREB1, SOS1, PRKAR2A, PRKACB, MAPK1, MAPK14, CAMK2D, and PRKAR1A, the OS of patients was longer than that in the relatively low-expression

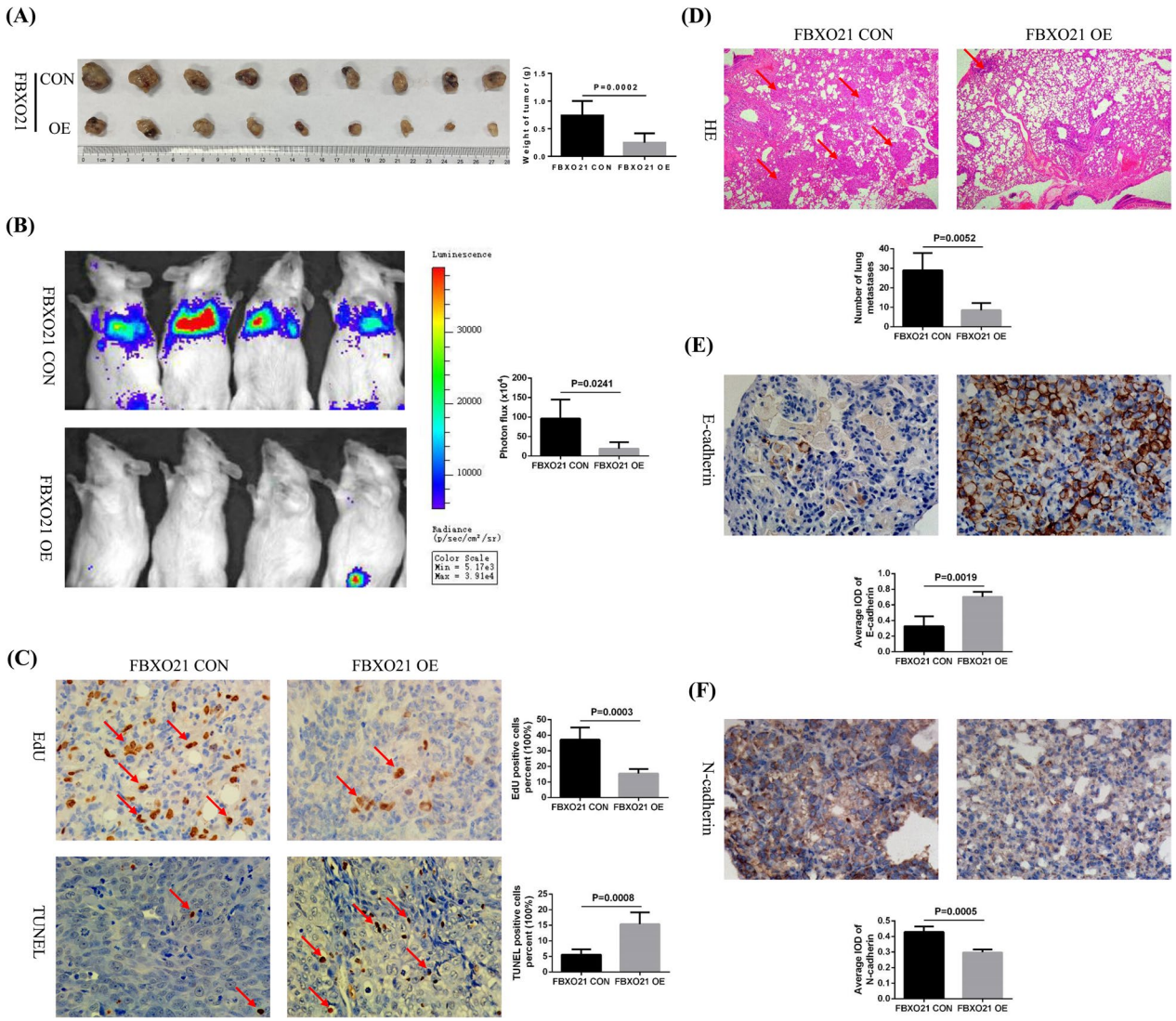

Fig. 5 Elucidate the effects of FBXO21 overexpression on the growth and lung metastasis of ccRCC cells in vivo. **A** Effects of FBXO21 overexpression on the growth of ccRCC cells. **B** Effects of FBXO21 overexpression on the lung metastasis of ccRCC cells. **C** Effects of FBXO21 overexpression of on EdU expression in mouse renal tumors. **D** Effects of FBXO21 overexpression of on TUNEL expression in mouse renal tumors. **E** Effects of FBXO21 overexpression on E-cadherin expression in pulmonary metastatic tumors. **F** Effects of FBXO21 overexpression on N-cadherin expression in pulmonary metastatic tumors

groups (Fig. 7C). In the group with higher expression of RPS6KA5, CREB1, SOS1, PRKAR2A, PRKACB, MAPK1, CAMK2D, and PRKAR1A, the RFS of patients was also longer (Fig. 7D).

Furthermore, we used immunofluorescence to detect the sublocalization of FBXO21 expression in ccRCC and AN tissues, and TOMM20 protein located on the outer membrane of the mitochondria was used as a cytoplasmic marker. The results confirmed that FBXO21 was expressed mainly in the cytoplasm (red) (Fig. 8A). Finally, we used Western blot to detect the expression of these key molecules in FBXO21-overexpressing cells and control cells. Our results confirmed that FBXO21 overexpression significantly promoted the protein expression of CREB1, SOS1, CAMK2D, PRKACB, MAPK1, PRKAR2A, and PRKAR1A in the OSRC2 and Caki-1 cell lines (Fig. 8B and C).

Therefore, our above results suggest that FBXO21 may regulate the CREB pathway and is involved in the infiltration of tumor immune cells in ccRCC.

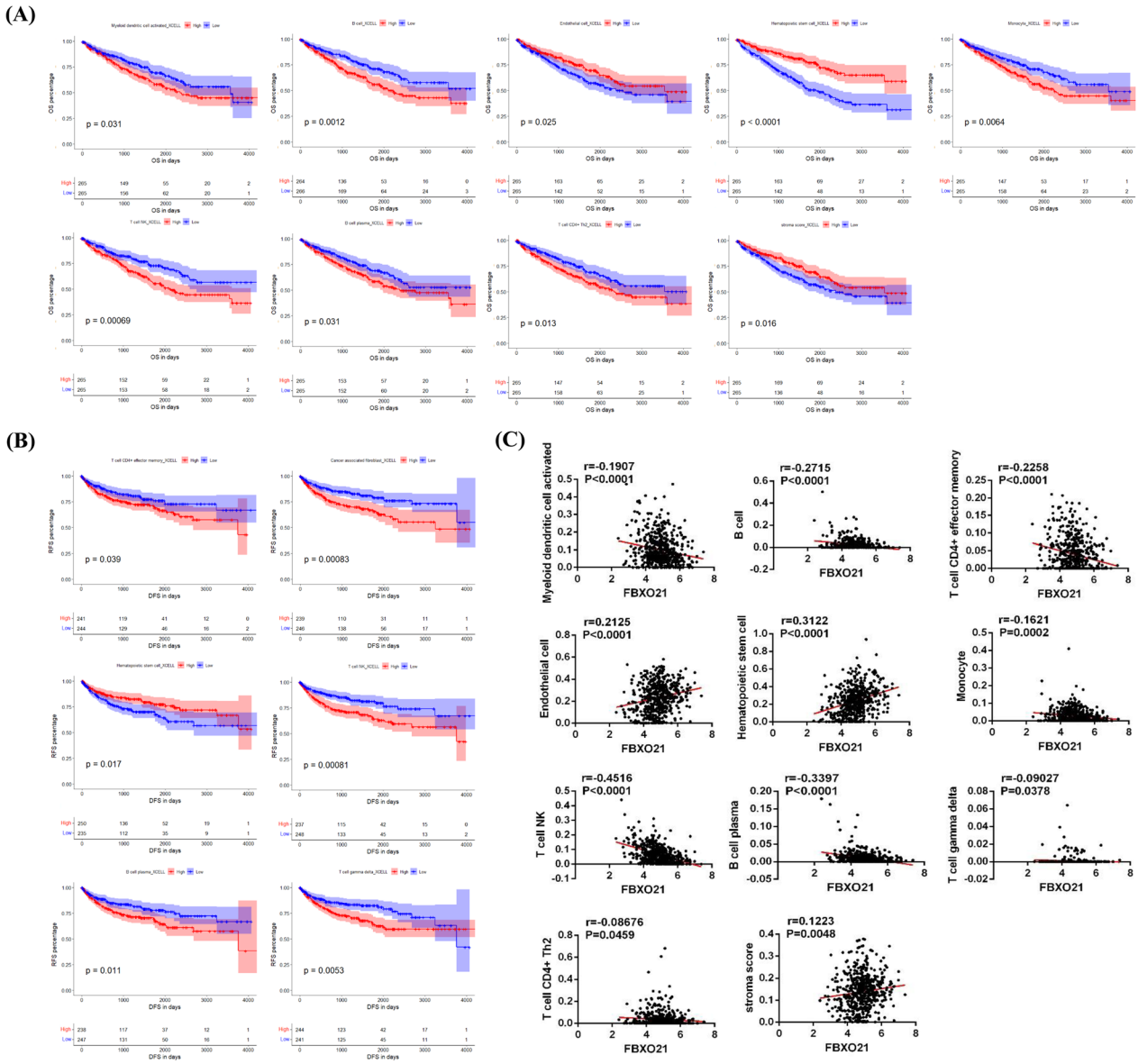

Fig. 6 Analysis of the relationship between FBXO21 expression and the infiltration levels of tumor immune cells in ccRCC. **A** Relationships between the infiltration levels of tumor immune cells and the OS of patients. **B** Relationships between the infiltration levels of tumor immune cells and the RFS of patients. **C** Correlation between the infiltration levels of tumor immune cells with prognostic significance and the expression of FBXO21. *OS* overall survival, *RFS* recurrence free survival

Discussion

At present, there is limited research on FBXO21 in tumors, with only a few studies indicating its potential role in gastric cancer and acute myeloid leukemia (AML). For example, FBXO21 expression is reduced in gastric cancer tissue and significantly correlated with poor patient prognosis, and FBXO21 inhibits the progression of gastric cancer by inducing growth arrest and suppressing cell migration and invasion [21]. FBXO21 is expressed at low levels in AML, but patients with high FBXO21 expression have a poor prognosis, and silencing FBXO21 in human AML cell lines and primary patient samples leads to differentiation, inhibition of tumor progression, and sensitization to chemotherapy drugs [22]. Consistent with the above two research results, we also found that FBXO21 expression was significantly reduced in ccRCC tissues and cell lines in this study, and that low FBXO21 expression was closely related to shorter OS and RFS in patients. Besides, our in vitro cell phenotype experiments and in vivo animal experiments confirmed that FBXO21

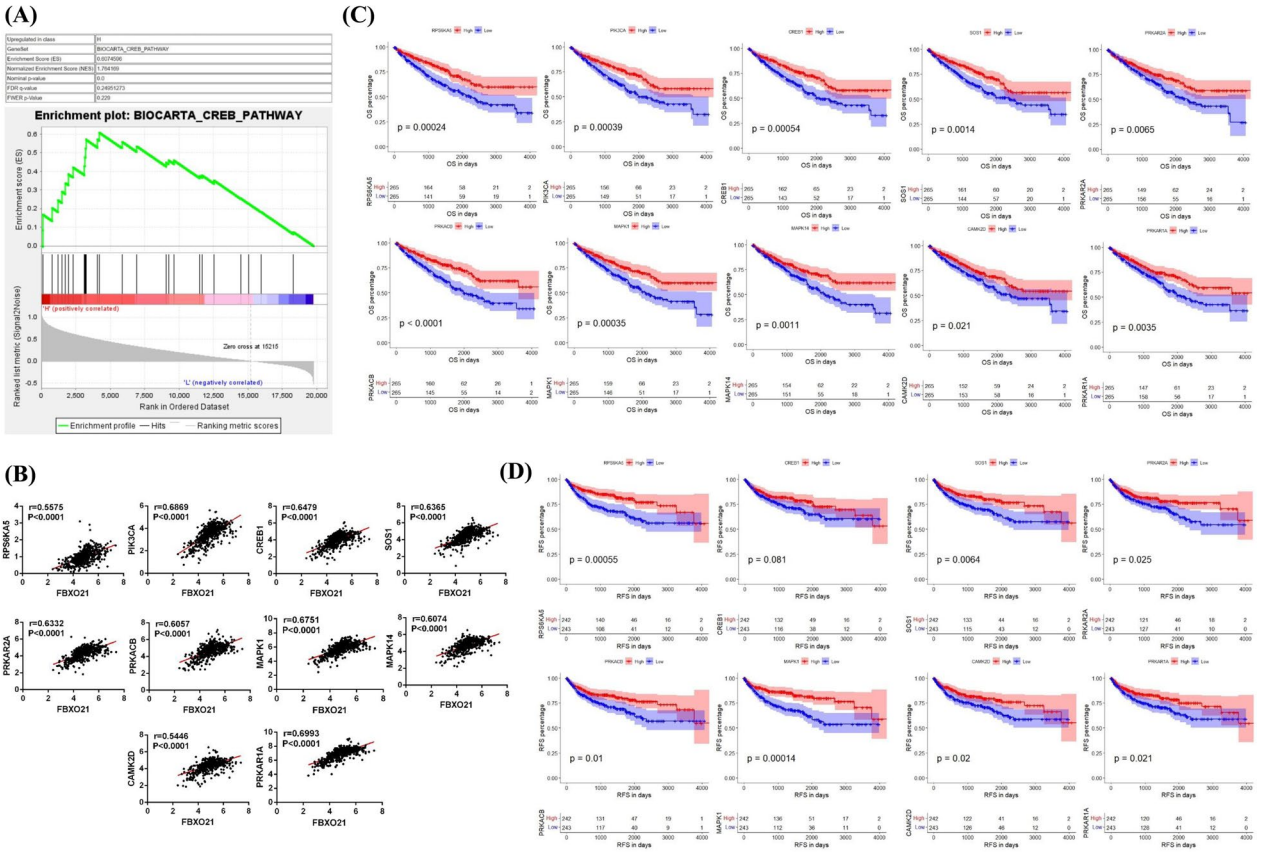

Fig. 7 GSEA of the FBXO21 high-expression group and low-expression group. **A** FBXO21 expression is closely related to the CREB pathway. **B** The correlation between the expression of key molecules in the CREB pathway and the expression of FBXO21. **C** The relationship between the expression of key molecules in the CREB pathway and the OS of patients. **D** Relationship between the expression of key molecules in the CREB pathway and the RFS of patients. *GSEA* Gene Set Enrichment Analysis, *OS* overall survival, *RFS* recurrence free survival

overexpression significantly inhibited the proliferation and metastasis ability of ccRCC cells and promoted cell apoptosis. Therefore, our results demonstrated that FBXO21 may act as a tumor suppressor gene in ccRCC.

Recent studies have shown that as one of the modalities of epigenetic modification, the DNA hypermethylation state is frequently observed in ccRCC and is associated with poor prognosis in ccRCC patients [23, 24]. In addition, the expression of many tumor suppressor genes is silenced due to hypermethylation of their promoters [25–27]. Some studies have also indicated that high FBXO32 expression is associated with improved OS in esophageal cancer patients and that knocking out DNA methyltransferase-1 (DNMT1) in esophageal cancer cells increases the expression of FBXO32 and suppresses the growth and metastasis of tumors in mice [28]. Besides, high FBXO32 expression was associated with improved OS in glioma patients, and knockout of DNMT1 in glioma cells increased the FBXO32 expression and inhibited the malignant phenotype [29]. Our study revealed that the DNA methylation level of FBXO21, an F-box family protein, was significantly greater in ccRCC tissues than in AN tissues through bioinformatics analysis and pyrosequencing and that the FBXO21 protein expression level was significantly increased after demethylation drug treatment.

Recent advances in the study of the immune checkpoint receptors, CTLA-4 and PD-1 in cancer immunogenicity and their inhibition have prompted a shift in thinking about cancer treatment strategies [30]. Therefore, a better understanding of the tumor immune microenvironment (TIME) will contribute to the selection of tumor immunotherapy methods. The TIME is composed of various immune and non-immune cells, including T cells, B cells, NK cells, DCs, macrophages, MDSCs, fibroblasts, and endothelial cells, which interact with each other through a complex signalling pathway network and with tumor cells [31, 32]. In ccRCC, the TIME is complex and dynamic and involves both immunostimulatory and immunosuppressive factors. For example, tumor infiltrating lymphocytes are closely related to a better prognosis

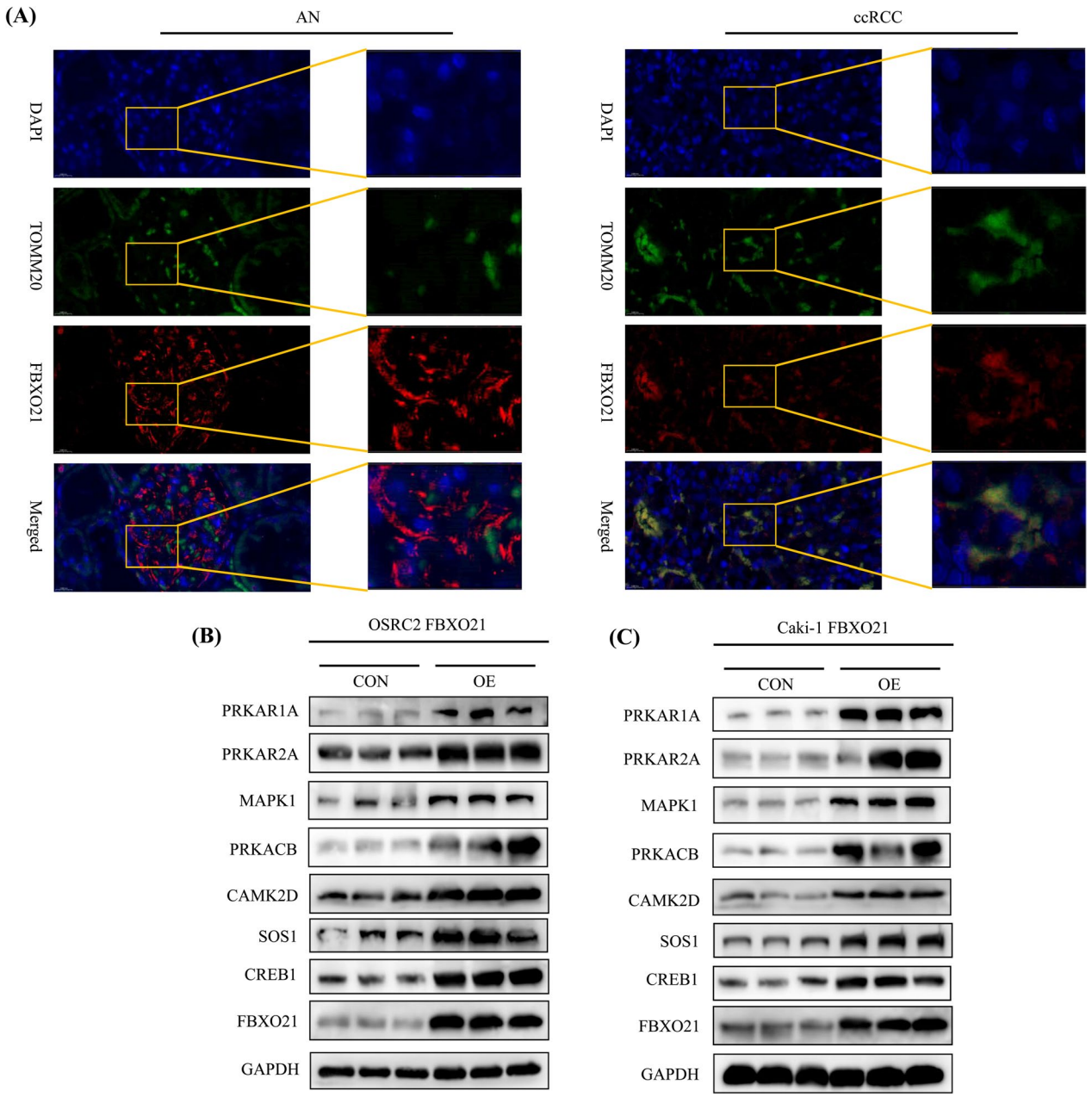

Fig. 8 Validation of the effects of FBXO21 overexpression on the expression of key molecules in the CREB pathway. **A** Sublocalization of FBXO21 protein expression (red) in ccRCC and AN tissues by immunofluorescence, TOMM20 protein (green) as a cytoplasmic marker. (**B** and **C**) Western blot anslysis of the expression of key proteins in the CREB pathway in FBXO21-overexpressing and control OSRC2 and Caki-1 cells. *AN* adjacent normal

in ccRCC patients, whereas high-density MDSCs inhibit anti-tumor immune responses [33]. Our analysis revealed that FBXO21 expression was significantly correlated with the stroma score and that the infiltration levels of 10 types of immune infiltrating cells (Myeloid dendritic cell activated, B cell, T cell CD4+effector memory, Endothelial cell, Hematopoietic stem cell, Monocyte, T cell NK, B cell plasma, T cell gamma delta, and T cell CD4+Th2) associated with prognosis. In addition, the GSEA results indicated that FBXO21 expression was closely related to the CREB pathway, and the CREB pathway was significantly activated in the high FBXO21 expression group. Moreover, we validated the regulatory effect of FBXO21 overexpression on the expression of key molecules in the CREB pathway via Western blot.

Interestingly, many studies have indicated that the CREB pathway is closely related to tumor-infiltrating immune cells [34–36]. Therefore, we speculated that FBXO21 likely achieves tumor suppression by regulating the CREB pathway to affect the infiltration level of related immune cells in ccRCC. However, to verify this hypothesis, further in-depth research is needed in the near future. First, the specific regulatory mechanism by which FBXO21 affects the CREB pathway needs further exploration. Second, although our results revealed a close correlation between FBXO21 expression and the infiltration levels of tumor immune cells and the CREB pathway has also been reported to regulate tumor immune cell infiltration, the specific relationship between them still needs further clarification by more in vitro and in vivo experiments.

Taken together, in this study, we found that the expression of FBXO21 and the methylation level of its CpG site, cg12414070, were strongly correlated with OS and RFS in patients with ccRCC and thus can be used as prognostic markers for ccRCC patients. However, this still needs to be validated in more clinical samples. In addition, we confirmed the tumor inhibitory effect of FBXO21 in ccRCC, and further exploration of its regulatory effect and mechanism on tumor immune cell infiltration and the CREB pathway in the near future will help identify new therapeutic targets for kidney cancer and promote the development of new therapeutic drugs. In addition, although this study selected the FBXO21 molecule as the research object through public database screening and clinical sample validation, the role of other molecules in the F-box protein family in ccRCC should not be ignored.

Conclusions

Taken together, the results of this study confirmed the low expression of FBXO21 in ccRCC, and promoter hypermethylation was an important reason for its reduced expression. In addition, FBXO21 overexpression significantly inhibited the proliferation and metastasis ability of ccRCC cells both in vitro and in vivo. Finally, we found that FBXO21 may regulate the CREB pathway and is closely related to tumor immune cell infiltration.

Abbreviations

RCC	Renal cell carcinoma
ccRCC	Clear cell RCC
VEGF	Vascular endothelial growth factor
mRCC	Metastatic RCC
EMT	Epithelial–mesenchymal transition
TCGA-KIRC	The cancer genome atlas-kidney renal clear cell carcinoma
GEO	Gene expression omnibus
GSEA	Gene set enrichment analysis
OS	Overall survival
RFS	Recurrence free survival
5-Aza	5-Azacytidine
DNMT1	DNA methyltransferase-1
AML	Acute myeloid leukemia
TIME	Tumor immune microenvironment

Supplementary Information

The online version contains supplementary material available at https://doi.org/10.1186/s12967-025-06356-y.

Supplementary file 1. Figure 1. Expression of F-box proteins in ccRCC and AN tissues on the basis of TCGA-KIRC data.Heatmap.Comparative analysis results. AN: adjacent normal

Supplementary file 2. Figure 2. Relationships between the expression of F-box proteins and the OS of ccRCC patients on the basis of TCGA-KIRC data. OS: overall survival

Supplementary file 3. Figure 3. Relationships between the expression of F-box proteins and RFS in ccRCC patients according to TCGA-KIRC data. RFS: recurrence free survival

Supplementary file 4. Figure 4. Relationships between FBXO15, FBXO21, and FBXO43 expression and the clinicopathological characteristics of ccRCC patients according to TCGA-KIRC data.Comparison of FBXO15, FBXO21, and FBXO43 expression between T1/T2 and T3/T4 tumors, G1/G2 and G3/G4 tumors, Stage I/II and Stage III/IV tumors, and M0 and M1 tumors.Comparison of FBXO43 expression between N0 and N1 tumors. M0: without distant metastasis, M1: with distant metastasis, N0: without lymph node invasion, N1: with lymph node invasion

Supplementary file 5. Figure 5. Validation of the expression of FBXO15, FBXO21, and FBXO43 in ccRCC and their clinical significance on the basis of GEO data.Comparison of FBXO15, FBXO21 and FBXO43 expression between ccRCC and AN tissues on the basis of data from 8 datasets. Comparison of FBXO15, FBXO21, and FBXO43 expression between Stage I/II and Stage III/IV tumors, G1/G2 and G3/G4 tumors, and M0 and M1 tumors. M0: without distant metastasis, M1: with distant metastasis. AN: adjacent normal

Supplementary file 6. Figure 6. Representative pyrosequencing peak maps of ccRCC and AN tissues. AN: adjacent normal

Supplementary file 7. Table 1: Sample collection information of 120 ccRCC patients

Acknowledgements

Not applicable.

Author contributions

WPY: Designed and implemented the experiments, collected and analysed the data, and wrote and revised the manuscript. TLJ and CJW: Collected tumor samples and followed-up with patients. MHL and XLY: Collected and analysed the data. DP and DX: Designed the experiments, provided funding support and revised the manuscript. All the authors have read and approved the final version of the manuscript.

Funding

This work was supported by Zhejiang Provincial Natural Science Foundation of China under Grant No. LQ23H160027 and ZCLQN25H1608 and the National Natural Science Foundation of China under Grant No. 82303143.

Availability of data and materials

All the data analysed and generated in this study are included in this manuscript.

Declarations

Ethics approval and consent to participate

This study was approved by the First Affiliated Hospital, Zhejiang University School of Medicine, Hangzhou, China, and we have obtained informed consent signed by all patients or their families (Ethical approval number: 2024 Research No. 0921).

Consent for publication

Not applicable.

Competing interests

The authors declare that they have no competing interests.

Author details

[1]Department of Urology, the First Affiliated Hospital, Zhejiang University School of Medicine, 79 Qingchun Road, Hangzhou 310003, Zhejiang, People's Republic of China.

Received: 4 November 2024 Accepted: 8 March 2025
Published online: 15 March 2025

References

1. Bray F, Laversanne M, Sung H, Ferlay J, Siegel RL, Soerjomataram I, et al. Global cancer statistics 2022: GLOBOCAN estimates of incidence and mortality worldwide for 36 cancers in 185 countries. Cancer J Clin. 2024;74(3):229–63. https://doi.org/10.3322/caac.21834.
2. Siegel RL, Giaquinto AN, Jemal A. Cancer statistics, 2024. Cancer J Clin. 2024;74(1):12–49. https://doi.org/10.3322/caac.21820.
3. Montemagno C, Jacquel A, Pandiani C, Rastoin O, Dawaliby R, Schmitt T, et al. Unveiling CXCR2 as a promising therapeutic target in renal cell carcinoma: exploring the immunotherapeutic paradigm shift through its inhibition by RCT001. J Exp Clin Cancer Res CR. 2024;43(1):86. https://doi.org/10.1186/s13046-024-02984-2.
4. Choueiri TK, Motzer RJ. Systemic therapy for metastatic renal-cell carcinoma. N Engl J Med. 2017;376(4):354–66. https://doi.org/10.1056/NEJMra1601333.
5. Ingels A, Campi R, Capitanio U, Amparore D, Bertolo R, Carbonara U, et al. Complementary roles of surgery and systemic treatment in clear cell renal cell carcinoma. Nat Rev Urol. 2022;19(7):391–418. https://doi.org/10.1038/s41585-022-00592-3.
6. Tur J, Webster RM. The renal cell carcinoma drug market. Nat Rev Drug Discov. 2024;23(1):16–7. https://doi.org/10.1038/d41573-023-00186-7.
7. Jonasch E, Gao J, Rathmell WK. Renal cell carcinoma. BMJ Clin Res. 2014;349: g4797. https://doi.org/10.1136/bmj.g4797.
8. Roskoski R Jr. Combination immune checkpoint and targeted protein kinase inhibitors for the treatment of renal cell carcinomas. Pharmacol Res. 2024;203: 107181. https://doi.org/10.1016/j.phrs.2024.107181.
9. Chatwal MS, Chahoud J, Spiess PE. Revisiting mechanisms of resistance to immunotherapies in metastatic clear-cell renal-cell carcinoma. Cancer drug Resist. 2023;6(2):314–26. https://doi.org/10.20517/cdr.2023.09.
10. Borcherding N, Vishwakarma A, Voigt AP, Bellizzi A, Kaplan J, Nepple K, et al. Mapping the immune environment in clear cell renal carcinoma by single-cell genomics. Commun biol. 2021;4(1):122. https://doi.org/10.1038/s42003-020-01625-6.
11. Raimondi A, Randon G, Sepe P, Claps M, Verzoni E, de Braud F, et al. The evaluation of response to immunotherapy in metastatic renal cell carcinoma: open challenges in the clinical practice. Int J Mol Sci. 2019. https://doi.org/10.3390/ijms20174263.
12. Díaz VM, de Herreros AG. F-box proteins: keeping the epithelial-to-mesenchymal transition (EMT) in check. Semin Cancer Biol. 2016;36:71–9. https://doi.org/10.1016/j.semcancer.2015.10.003.
13. Sun C, Tao Y, Gao Y, Xia Y, Liu Y, Wang G, et al. F-box protein 11 promotes the growth and metastasis of gastric cancer via PI3K/AKT pathway-mediated EMT. Biomed Pharmacother Biomedine Pharmacother. 2018;98:416–23. https://doi.org/10.1016/j.biopha.2017.12.088.
14. Sun R, Xie HY, Qian JX, Huang YN, Yang F, Zhang FL, et al. FBXO22 possesses both protumorigenic and antimetastatic roles in breast cancer progression. Can Res. 2018;78(18):5274–86. https://doi.org/10.1158/0008-5472.can-17-3647.
15. Liu K, Xue B, Bai G, Zhang W. F-box protein FBXO31 modulates apoptosis and epithelial-mesenchymal transition of cervical cancer via inactivation of the PI3K/AKT-mediated MDM2/p53 axis. Life Sci. 2020;259: 118277. https://doi.org/10.1016/j.lfs.2020.118277.
16. Wu J, Wen T, Marzio A, Song D, Chen S, Yang C, et al. FBXO32-mediated degradation of PTEN promotes lung adenocarcinoma progression. Cell Death Dis. 2024;15(4):282. https://doi.org/10.1038/s41419-024-06635-4.
17. Fan B, Wang W, Zhang X, Sun M, Wang X, Chen Z, et al. Prevalence and prognostic value of FBXO11 expression in patients with clear cell renal cell carcinoma. BMC Cancer. 2019;19(1):534. https://doi.org/10.1186/s12885-019-5736-8.
18. Yuan Y, Liu Z, Li B, Gong Z, Piao C, Liu Z, et al. FBXO30 functions as a tumor suppressor and an E3 ubiquitin ligase for hZIP1-mediated HIF-1α degradation in renal cell carcinoma. Int J Oncol. 2023. https://doi.org/10.3892/ijo.2023.5488.
19. Yang W, Zhou J, Zhang Z, Zhang K, Xu Y, Li L, et al. Downregulation of lncRNA APCDD1L-AS1 due to DNA hypermethylation and loss of VHL protein expression promotes the progression of clear cell renal cell carcinoma. Int J Biol Sci. 2022;18(6):2583–96. https://doi.org/10.7150/ijbs.71519.
20. Yang W, Zhang K, Zhang Z, Zhou J, Li L, Xu Y, et al. Claudin-10 overexpression suppresses human clear cell renal cell carcinoma growth and metastasis by regulating ATP5O and causing mitochondrial dysfunction. Int J Biol Sci. 2022;18(6):2329–44. https://doi.org/10.7150/ijbs.70105.
21. Jiang Y, Liu X, Shen R, Gu X, Qian W. Fbxo21 regulates the epithelial-to-mesenchymal transition through ubiquitination of Nr2f2 in gastric cancer. J Cancer. 2021;12(5):1421–30. https://doi.org/10.7150/jca.49674.
22. Dobish KK, Wittorf KJ, Swenson SA, Bean DC, Gavile CM, Woods NT, et al. FBXO21 mediated degradation of p85α regulates proliferation and survival of acute myeloid leukemia. Leukemia. 2023;37(11):2197–208. https://doi.org/10.1038/s41375-023-02020-w.
23. Comprehensive molecular characterization of clear cell renal cell carcinoma. Nature. 2013; 499 7456: 43–9. https://doi.org/10.1038/nature12222.
24. Joosten SC, Smits KM, Aarts MJ, Melotte V, Koch A, Tjan-Heijnen VC, et al. Epigenetics in renal cell cancer: mechanisms and clinical applications. Nat Rev Urol. 2018;15(7):430–51. https://doi.org/10.1038/s41585-018-0023-z.
25. Baylin SB, Jones PA. Epigenetic determinants of cancer. Cold Spring Harb Perspect Biol. 2016. https://doi.org/10.1101/cshperspect.a019505.
26. Krassenstein R, Sauter E, Dulaimi E, Battagli C, Ehya H, Klein-Szanto A, et al. Detection of breast cancer in nipple aspirate fluid by CpG island hypermethylation. Clin Cancer Res. 2004;10(1 Pt 1):28–32. https://doi.org/10.1158/1078-0432.ccr-0410-3.
27. Miyakuni K, Nishida J, Koinuma D, Nagae G, Aburatani H, Miyazono K, et al. Genome-wide analysis of DNA methylation identifies the apoptosis-related gene UQCRH as a tumor suppressor in renal cancer. Mol Oncol. 2022;16(3):732–49. https://doi.org/10.1002/1878-0261.13040.
28. Song XQ, Chen BB, Jin YM, Wang CY. DNMT1-mediated epigenetic suppression of FBXO32 expression promoting cyclin dependent kinase 9 (CDK9) survival and esophageal cancer cell growth. Cell cycle (Georgetown, Tex). 2024;23(3):262–78. https://doi.org/10.1080/15384101.2024.2309022.
29. Quan J, Ma C. DNMT1-mediated regulating on FBXO32 promotes the progression of glioma cells through the regulation of SKP1 activity. Environ Toxicol. 2024;39(2):783–93. https://doi.org/10.1002/tox.23976.
30. Monjaras-Avila CU, Lorenzo-Leal AC, Luque-Badillo AC, D'Costa N, Chavez-Muñoz C, Bach H. The tumor immune microenvironment in clear cell renal cell carcinoma. Int J Mol Sci. 2023. https://doi.org/10.3390/ijms24097946.
31. Hanahan D, Weinberg RA. Hallmarks of cancer: the next generation. Cell. 2011;144(5):646–74. https://doi.org/10.1016/j.cell.2011.02.013.
32. Gubin MM, Esaulova E, Ward JP, Malkova ON, Runci D, Wong P, et al. High-Dimensional analysis delineates myeloid and lymphoid compartment remodeling during successful immune-checkpoint cancer

therapy. Cell. 2018;175(4):1014-30.e19. https://doi.org/10.1016/j.cell.2018.09.030.
33. Hakimi AA, Voss MH, Kuo F, Sanchez A, Liu M, Nixon BG, et al. Transcriptomic profiling of the tumor microenvironment reveals distinct subgroups of clear cell renal cell cancer: data from a randomized phase III trial. Cancer Discov. 2019;9(4):510–25. https://doi.org/10.1158/2159-8290.cd-18-0957.
34. Lin W, Szabo C, Liu T, Tao H, Wu X, Wu J. STING trafficking activates MAPK-CREB signaling to trigger regulatory T cell differentiation. Proc Natl Acad Sci USA. 2024;121(29): e2320709121. https://doi.org/10.1073/pnas.2320709121.
35. Yan C, Yang Z, Chen P, Yeh Y, Sun C, Xie T, et al. GPR65 sensing tumor-derived lactate induces HMGB1 release from TAM via the cAMP/PKA/CREB pathway to promote glioma progression. J Exp Clin Cancer Res: CR. 2024;43(1):105. https://doi.org/10.1186/s13046-024-03025-8.
36. Masjedi A, Hassannia H, Atyabi F, Rastegari A, Hojjat-Farsangi M, Namdar A, et al. Downregulation of A2AR by siRNA loaded PEG-chitosan-lactate nanoparticles restores the T cell mediated anti-tumor responses through blockage of PKA/CREB signaling pathway. Int J Biol Macromol. 2019;133:436–45. https://doi.org/10.1016/j.ijbiomac.2019.03.223.

Publisher's Note